nature communications

Article

https://doi.org/10.1038/s41467-025-67544-4

Designing an oxidase toolbox for site-directed oxidation of taxanes

Received: 1 February 2025

Accepted: 3 December 2025

Published online: 17 December 2025

Check for updates

Mingyuan Lai[1], Yu Weng[1], Jian Wei[1], Xin-Yi Lu[1], Zhengyu Huang[1], Hangcheng Li[1], Longhao Huang[1], Zhijun Zhang[1], Lili Zhu[2], Jian-He Xu[1], Ran Hong[2] & Hui-Lei Yu[1]

Paclitaxel is one of the most prominent drugs for cancer therapy, and its synthesis has long been pursued by scientific community. Although the biosynthetic pathway has been gradually unraveled, its synthetic efficiency remains severely constrained by the low activity and low product selectivity of the hydrolases involved. In this study, an artificial toolbox of oxidases derived from mutants of *Tte*UPO (unspecific peroxygenase from *Thielavia terrestris*) is developed for site-directed oxidation of taxanes at the C-4, C-6, C-10, C-11, C-12, and C-13 positions. Furthermore, de novo biosynthesis of oxidized taxadiene products is achieved in an engineered *E. coli* chassis. These findings offer an unconventional strategy for developing an efficient route toward paclitaxel and constructing paclitaxel analogs with different structures for medicinal evaluation.

Paclitaxel (Taxol®), a tetracyclic and functionally condensed diterpenoid, is renowned for its extensive anticancer efficacy. Its structural derivatives are widely utilized in the treatment of various malignancies (Fig. 1)[1]. Docetaxel and cabazitaxel, both classified alongside paclitaxel as first-generation taxane anticancer drugs, have therapeutic applications distinct from those of paclitaxel[2,3]. Next-generation taxoids feature modifications to the critical sites of paclitaxel, including the functional groups at C-10 and C-13. Notably, compounds such as SB-T-1214 have demonstrated remarkable efficacy against drug-resistant tumors[4–6].

Paclitaxel is produced primarily *via* a semisynthetic method. Initial, 10-deacetyl-baclitatin III (10-DAB) is extracted from the needles of *Taxus baccata* L., after which its side chain is assembled through a 4-step chemical process[7,8]. Although this method has significantly improved the yield of paclitaxel compared with direct extraction from the bark of *Taxus brevifolia* Nutt.[9–11], the clinical demand remains unfulfilled due to the long growth cycle and limited bioresources. The chemical synthesis of paclitaxel and its analogs has witnessed rapid advancements, yet challenges such as lengthy synthetic steps and low overall yields persist[12–17].

In recent years, substantial progress has been made in elucidating and optimizing the natural biosynthetic pathway of paclitaxel, and all enzymes involved have been identified[18–28]. In 2010, the yield of taxadiene, the crucial paclitaxel precursor, produced by designed *Escherichia coli* cells was increased to 1 g/L[18]. The downstream biosynthetic of paclitaxel is severely limited by the low activity and low product selectivity of the cytochrome P450 monooxygenases (P450s) involved in native taxadiene oxidative derivation steps[29–31]. Despite the progress in elucidating the mechanism of taxadiene-5α-hydroxylase (T5αH), as the native enzyme responsible for the initial step in taxadiene oxidation, efforts to substantially enhance its catalytic efficiency and specificity *via* protein engineering have thus far proven unsuccessful[32–34]. To overcome the inherent limitations of T5αH, Xiao et al. investigated alternative taxadiene-oxidizing enzymes, finding that although CYP701A8 mediates C11-position oxidation, its application is severely constrained by pronounced allosteric effects[35]. Notably, Zhang et al. established the complete gene set requisite for heterologous paclitaxel biosynthesis and identified a taxadiene-epoxidizing enzyme that synergizes with T5αH to facilitate oxetane ring formation[19]. McClune et al. discovered FoTO1, an NTF2-like protein, can resolved the low product selectivity of T5αH, suppressing byproduct formation (e.g., OCT) and enabling the selective production of taxadiene-5α-ol (T5OH). This approach

[1]State Key Laboratory of Bioreactor Engineering, Shanghai Collaborative Innovation Centre for Biomanufacturing, East China University of Science and Technology, Shanghai, PR China. [2]State Key Laboratory of Chemical Biology, Shanghai Institute of Organic Chemistry, Chinese Academy of Sciences, Shanghai, PR China. e-mail: huileiyu@ecust.edu.cn

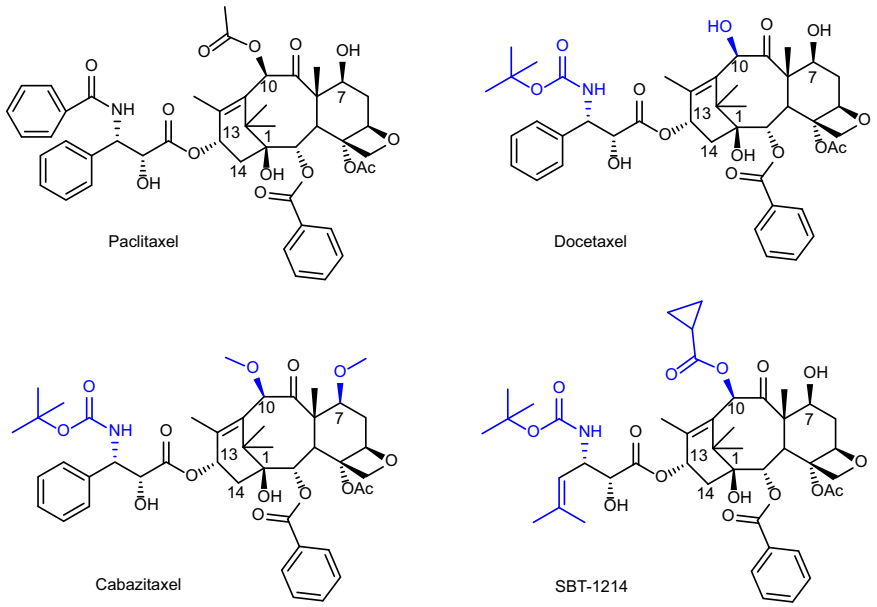

Fig. 1 | Paclitaxel and its structural derivatives. Structures of paclitaxel, docetaxel, cabazitaxel, and SBT-1214 are shown.

resulted in the isolation of baccatin III at ~8.7 μg/g DW from *N. benthamiana*[36].

In the present study, we focus on identifying non-native taxadiene oxidases as alternatives to the native P450 enzymes. *Tte*UPO (unspecific peroxygenase from *Thielavia terrestris*)[37,38] is selected from 29 fungal-originated oxidases because of its highest activity toward taxadiene and excellent protein expression level in *Pichia pastoris*. We construct an enzyme toolbox comprising various *Tte*UPO mutants, which exhibit distinct regioselectivities toward the taxadiene skeleton. Moreover, we engineer an *E. coli* BL21 (DE3) strain for the de novo biosynthesis of oxidized taxadiene products by introducing the taxadiene biosynthetic pathway and enabling the heterologous expression of a *Tte*UPO mutant. These results lay a solid foundation for future development of artificial synthetic routes to paclitaxel and its analogs.

Results

Mining and characterization of taxane oxidases

Peroxidases and peroxygenases, both featuring heme coordinated by a cysteine ligand similar to that of P450s[39–42], have been successfully utilized for the oxy-functionalization of carbon, sulfur, silicon, and nitrogen[43–47]. However, there are no reports of oxidases other than P450s that are capable of oxidizing taxanes. We initially screened 29 reported peroxidases and peroxygenases of fungal origin[37,38,48–54], which were expressed in *Pichia pastoris* (syn. *Komagataella phaffii*). Among these, 13 oxidases exhibited activity toward taxadiene, producing identical oxidation products. *Tte*UPO (unspecific peroxygenase from *Thielavia terrestris*)[37,38] was chosen due to its highest activity and excellent protein expression level (Supplementary Note 1, Supplementary Tables 1, 2 and Supplementary Fig. 1, 2). *Tte*UPO catalyzes the formation of hydroxylation products through the C-H activation of C-4 and C-6 positions in the taxadiene skeleton (Fig. 2A). Compounds **3** and **4** were identified as stereoisomers of the C-4 hydroxylation product ((*S*)-taxa-5(6),11(12)-dien-4-ol (**3**) and (*R*)-taxa-5(6),11(12)-diene-4-ol (**4**)), whereas **5** and **6** were found to be stereoisomers of the C-6 hydroxylation product ((*R*)-taxa-4(5),11(12)-diene-6-ol (**5**) and (*S*)-taxa-4(5),11(12)-dien-6-ol (**6**)). Additionally, during analysis of the given products by gas chromatography (GC), elimination of the allylic products resulted in a diene compound, namely, taxa-4(20),5(6),11(12)-triene (**2**) (Fig. 2B and Supplementary Fig. 3, 4, 5). This phenomenon was also observed when compounds **3** ~ **6** were dissolved in $CDCl_3$ and CD_2Cl_2 for NMR experiments, indicating a facile elimination process that is enhanced by heat and acidic conditions.

In contrast to the oxidation pattern of T5αH[17–20], *Tte*UPO catalyzed the oxidation of taxadiene to generate various hydroxylation substances that were distinct from byproducts such as OCT, iso-OCT or other compounds that constituted a large proportion of the products generated by T5αH in previous investigations[18,29,30] (Fig. 2C). The oxidation of taxadiene by *Tte*UPO was localized to either the C4 = C5 double bond or the allyl position of ring C. To elucidate the possible reaction pathway, taxadiene-4(5)-epoxide (**7**) was prepared by oxidation of taxadiene with DMDO[55,56] (Fig. 2C and Supplementary Fig. 6). This unstable epoxy intermediate undergoes spontaneous rearrangement to form the products T5OH, OCT, and iso-OCT[20,22,33,34]. In *Tte*UPO-catalyzed oxidation of taxadiene, taxadiene-4(5)-epoxide was not detected. Furthermore, epoxide **7** was not converted to compounds **3** ~ **6** by *Tte*UPO. These observations led us to conclude that *Tte*UPO-catalyzed taxadiene oxidation circumvents the taxadiene-4(5)-epoxide intermediate, thereby preventing the accumulation of byproducts (e.g., OCT). This finding also offers an alternative strategy to FoTO1 for addressing the McClune et al. discovered FoTO1, an NTF2-like protein, can resolved the low product selectivity of T5αH.

Protein engineering of *Tte*UPO

Next, the catalytic efficiency was enhanced by protein engineering. Interestingly, the regioselectivity of *Tte*UPO was also modified to enable oxidation at distinct sites of taxadiene. The crystal structure of *Tte*UPO (PDB 9IZ8) was analyzed at a high resolution of 1.54 Å (Supplementary Fig. 7 and Supplementary Table 3). The conformation of substrate channel has been found to substantially influence the activity and selectivity of UPOs[57–61]. Molecular docking was performed *via* AutoDock Vina[62], the fining docking structure indicates that the substrate channel of *Tte*UPO is narrowed due to excessive steric hindrance of amino acids within the channel, thereby restricting the entry and binding of taxadiene (Supplementary Fig. 8). Furthermore, given the minimal polarity and strong hydrophobicity of taxadiene, which prevents hydrogen bond formation with surrounding amino acids, amino acids lining the substrate channel were mutated to alanine (Ala)—a sterically less hindered nonpolar amino acid. These mutations widen the channel and identify sensitive residues for further precise regulation of the channel geometry (Supplementary Tables 4 and 5).

https://doi.org/10.1038/s41467-025-67544-4

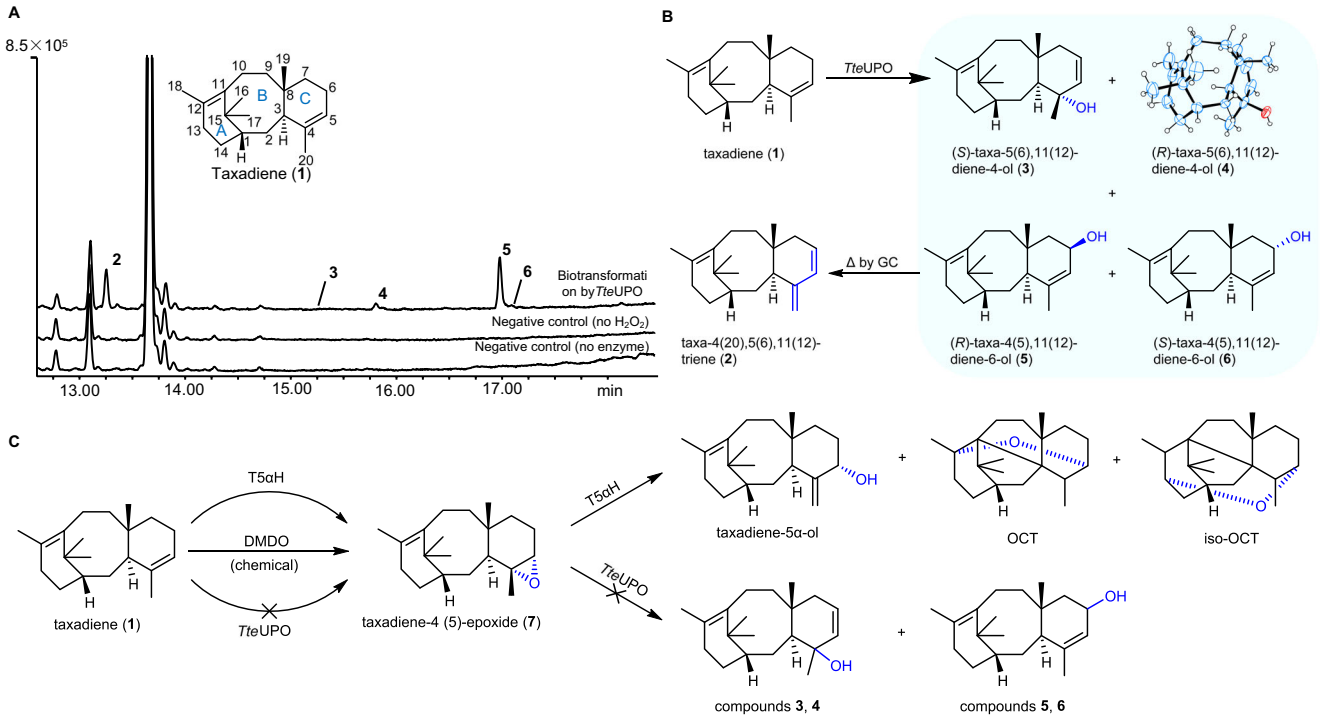

Fig. 2 | Products generated *via* *Tte*UPO-catalyzed oxidation of taxadiene. A GC analysis of the reaction catalyzed by *Tte*UPO. Compared to controls, five peaks (**2**-**6**) appeared in the *Tte*UPO reaction; **B** The enzymatic catalytic reaction formula and the chemical structures of all products generated *via* *Tte*UPO-catalyzed oxidation of taxadiene using ^{18}O-labeled H_2O_2. The structure of **4** was confirmed by X-ray crystallographic analysis (deposition number: 2374527) and drawn *via* ORTEP (Supplementary Fig. 5); **C** Comparative oxidation of taxadiene by T5αH, DMDO, and *Tte*UPO. Reaction pathway for T5αH proceeded as reported[71]. *Tte*UPO neither oxidized taxadiene to form compound **7** nor catalyzed the conversion of compound **7** (synthesized *via* DMDO) to downstream products.

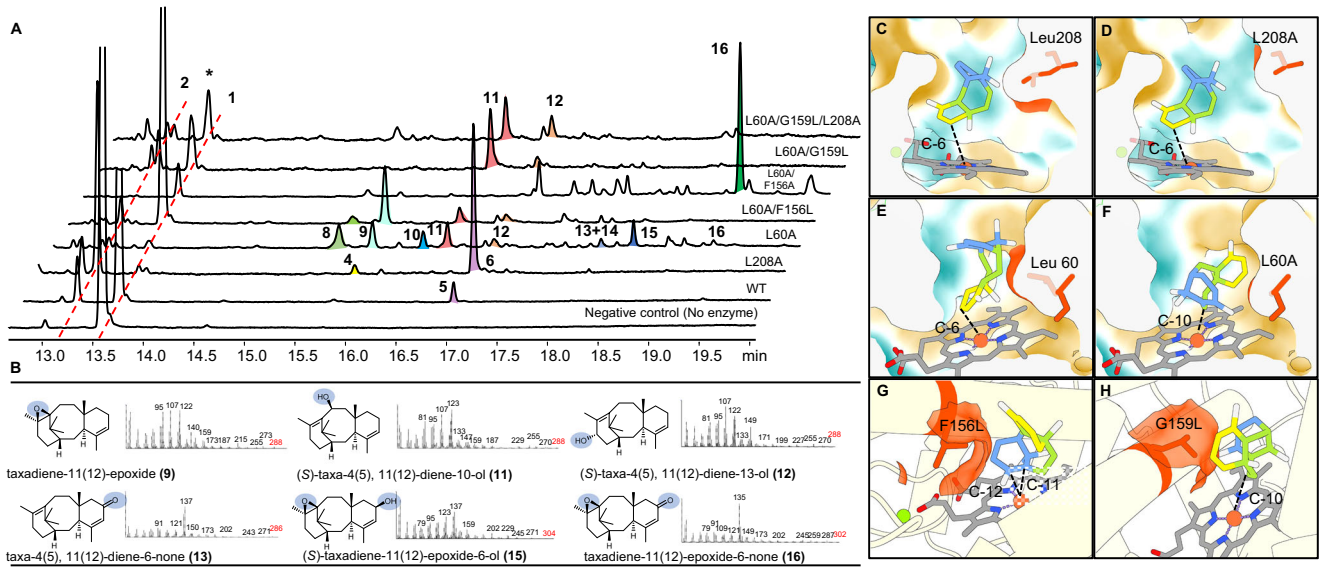

Fig. 3 | The oxidaiton products of taxadiene catalyzed by *Tte*UPO mutants and the structural distribution of the investigated mutations in *Tte*UPO. A GC analysis of taxadiene oxidation catalyzed by mutants of *Tte*UPO. * Under GC conditions, compounds **11** and **12** partially degrade, yielding products with retention times identical to taxadiene (**1**); **B** Structures and MS (EI) spectra of the identified products (**9, 11**-**13, 15**, and **16**). Compound **8** is the product generated by the thermal transformation of **15** during GC detection (Supplementary Fig. 15), upon scale-up, compounds **10** and **14** exhibited significantly diminished yields (Supplementary Fig. 9D); **C** Cross-sectional view of the *Tte*UPO (WT) structure, highlighting Leu208 (red); **D** Cross-sectional view of the L208A mutant structure, highlighting Ala208 (red); **E** Cross-sectional view of the *Tte*UPO (WT) structure, highlighting Leu60 (red); **F** Cross-sectional view of the L60A mutant structure, highlighting Ala60 (red); **G** Structure of the L60A/F156L mutant, highlighting Leu156 (red); **H** Structure of the L60A/G159L mutant, highlighting Leu159 (red). Color representation of taxadiene: blue for ring A, green for ring B and yellow for ring C.

The mutation of Leu208, which is located at the entrance of the substrate channel, to Ala, which results in less steric hindrance, widened the "bottle mouth". This modification facilitated the entry of taxadiene into the active center (Fig. 3C, D). The L208A mutant exhibited a significant improvement in catalytic activity, with no alteration in product diversity (Fig. 3A, Table 1 and Supplementary Fig. 9A, 9C). The total turnover number (TON) increased from 82 to 4355, a marked 53-fold increase.

https://doi.org/10.1038/s41467-025-67544-4

Table 1 | Comparison of the activity and selectivity of *Tte*UPO and its mutants for taxadiene oxidation

catalyst	Enzyme load (μg/mL)	TON[a]	Conv. (%)[b]	Product proportion (%)										
				3	4	5	6	9	11	12	13 + 14	15	16	Op[c]
WT	40	82	18.0 ± 0.7	<1	11	85	4	n.d.	n.d.	n.d.	n.d.	n.d.	n.d.	n.d.
L208A	4	4355	95.6 ± 0.5	1	12	85	2	n.d.	n.d.	n.d.	n.d.	n.d.	n.d.	n.d.
L60A	40	432	94.9 ± 0.4	n.d.	<1	4	n.d.	15	16	9	4	31	2	18
L60A/F156A	40	430	94.5 ± 0.7	n.d.	n.d.	n.d.	n.d.	2	n.d.	n.d.	10	6	51	31
L60A/F156L	40	224	49.2 ± 0.3	n.d.	n.d.	n.d.	n.d.	42	27	22	n.d.	8	n.d.	1
L60A/G159L	40	365	80.2 ± 0.2	n.d.	n.d.	2	n.d.	n.d.	66	19	2	n.d.	n.d.	11
L60A/G159L/L208A	20	757	83.1 ± 2.5	n.d.	n.d.	n.d.	n.d.	n.d.	41	33	2	n.d.	n.d.	24

[a]TONs were calculated for 1 h and are reported in units of $\mu mol_{substrate}$ converted μmol_{UPO}^{-1}.
[b]In a reaction involving 0.5 mM taxadiene.
[c]Other products. Source data are provided as a Source Data file.

Notably, the L60A mutant exhibited enhanced activity and demonstrated low product selectivity compared with the WT (Fig. 3A, B, Table 1 and Supplementary Fig. 9B, 9C). Leu60, which is positioned above the heme porphyrin ring, was substituted with alanine, thereby enhancing substrate accessibility to the catalytic site (Fig. 3E, F) and thus increasing its oxidative activity (Table 1). Moreover, expansion of the inner side of the substrate channel increases the diversity of the substrate binding conformations, resulting in the formation of more than 6 oxidation products (Fig. 3A, B). In contrast to the WT, the L60A mutant tended to attack the C11 = C12 double bond in ring A. In addition to the generation of hydroxylation products at the allylic positions (i.e., C-10 and C-13), epoxidation of the double bond in ring A was also observed, along with further oxidation of C-6 in ring C (Fig. 3A, B). Notably, the oxidation sites and configurations at C-10 and C-13 were identical to those in paclitaxel.

The L60S mutant exhibited activity and selectivity profiles comparable to those of L60A (Supplementary Fig. 9B). Although serine possesses a polar hydroxyl group not present in alanine, both residues impose similar steric constraints. This result further confirms that steric hindrance, rather than side-chain polarity, is the primary determinant of *Tte*UPO's activity and selectivity in taxadiene oxidation.

Interestingly, the L60A mutant exhibits remarkable versatility, catalyzing oxidations at the C-4, C-6, C-10, C-11, C-12, and C-13 positions of taxadiene. This renders it an excellent starting point for constructing a mutant library tailored to the regioselective oxidation of taxadiene. Mutants generated through FLA scanning (replaced with Phe, Leu, or Ala) and STY scanning (replaced with Ser, Thr, or Tyr)[63], along with site-directed saturation mutagenesis of amino acids within the substrate channel, were then specifically designed to enhance the regioselective oxidation capabilities of the mutant (Supplementary Fig. 10).

The combined mutant L60A/F156A enables catalysis of epoxidation at C-11 and C-12 and oxidation at C-6 on taxadiene, resulting in the formation of compound **16** (Table 1). Compared with the L60A/F156A mutant, the L60A/F156L mutant exhibits greater steric hindrance at position 156 due to the bulkier leucine residue replacing alanine. This increased steric clash further constrains the binding conformation of taxadiene and limits the positioning of ring C near heme-Fe. Additionally, the "concave surface" of taxadiene can only enter the active site with the concave side facing Leu156, positioning the double bond at ring A close to the heme-Fe (Fig. 3G and Supplementary Fig. 11C). As a result, the C-10 and C-13 hydroxylation products (compounds **11** and **12**), along with the C-11 and C-12 epoxidation product (compound **9**), dominate for over 90% of the products, while oxidation at C-6 occurs only rarely (Table 1).

Notably, the L60A/G159L mutant exhibited a significant increase in selectivity, specifically increasing the proportion of the C-10 (compounds **11**) and C-13 (compounds **12**) hydroxylation products to 66% and 19%, respectively, with a conversion of 80.2% (Table 1). In the presence of Leu159, which exhibits greater steric hindrance and thus constrains other substrate binding conformations, the substrate preferentially enters the channel with a parallel conformation relative to the heme plane. Consequently, ring B of taxadiene comes closest to heme-Fe, thereby favoring the hydroxylation product at C-10 of ring B. However, as the distance increases, the oxidation activity slightly deteriorates (Fig. 3H, Supplementary Fig. 11A, 11B, and Supplementary Table 6). To restore activity, the L60A/G159L mutant was combined with the activity-enhancing L208A mutation to generate the triple mutant L60A/G159L/L208A. This modification led to a significant performance improvement, achieving a turnover number (TON) of 757. Additionally, the selectivity for the hydroxylation product at C-13 was increased to 33% (Table 1). The L60A/G159L/L208A mutant also exhibited excellent scalability. In a 100 mL reaction system, the yield of 0.5 mM taxadiene catalyzed by 4 mg of enzyme reached 75.3% within 2 h.

Development of a taxane oxidase toolbox

Seven *Tte*UPO mutants were employed to construct an engineered oxidase toolbox, enabling site-specific oxidation of taxanes (Fig. 4A). Eleven distinct oxidized products were structurally characterized, revealing six oxidizable sites on the taxane scaffold (Fig. 4B and Supplementary Fig. 12). Compounds **11** and **12** exhibit regioselectivity and stereoselectivity consistent with those of paclitaxel, making them potential building blocks for reconstructing the paclitaxel synthesis pathway. Notably, the L60A/F156A and L60A mutants exhibit poor regioselectivity in catalyzing the oxidation of taxadiene. However, when additional steric hindrance is introduced at C-10 on ring B or C-4 on ring C of taxadiene (compound **11** and **4**), these mutants exhibit high regioselectivity in oxidizing taxanes, yielding compounds **17** and **18**. This highlights the versatility of the toolbox, which not only has been proven effective for taxadiene but also demonstrates even greater performance for taxadiene derivatives. The oxidation sites of compounds **5, 9, 13, 15, 16, 17**, and **18** differ from those of paclitaxel, and these distinct chemical modifications may result in diverse pharmacological activities, while oxidation at the C-6 position is associated with paclitaxel metabolism in the human body[64].

The biosynthesis of paclitaxel involves eight oxidative modifications of the taxadiene core structure (Fig. 1). The L208A mutant, which exhibits the highest activity, was employed to probe the oxidation capabilities of this engineered enzyme toolbox toward higher-oxidation-state taxane derivatives (compounds **19**/**21**/**23**) (Fig. 4 and Supplementary Fig. 12). The introduction of a C2-carbonyl group in compound **19** (*vs.* taxadiene) dramatically enhances both regioselectivity and stereoselectivity in L208A catalysis, with compound **20** accounting for over 99% of the total products. L208A selectively oxidizes the configurationally inverted isomer **21** to compound **22**, but shows no activity toward its stereoisomer **23**. We ultimately achieved the synthesis of tri-oxygenated taxanes, demonstrating the potential of our established enzyme toolbox to generate high oxidation state taxane derivatives.

https://doi.org/10.1038/s41467-025-67544-4

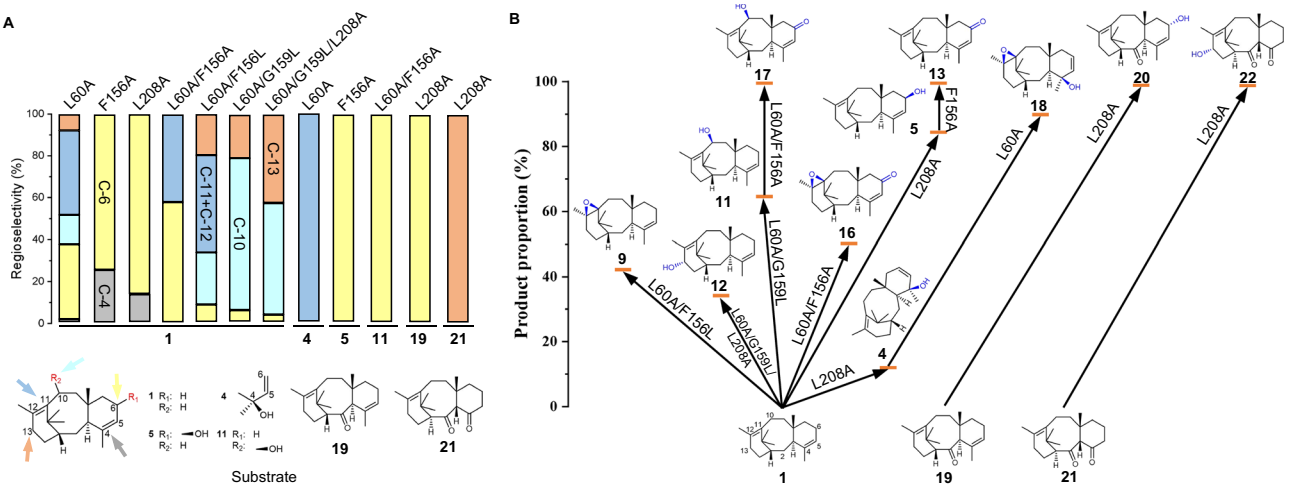

Fig. 4 | Design *Tte*UPO mutant's toolbox for functional oxidation of taxadiene and taxanes with diverse oxidation states. A Regioselectivity of mutants in the toolbox toward different taxanes. Definition of Regioselectivity: The peak area ratio between oxidation products at different positions on the taxane skeleton. Compound **15** or **16** is equally allocated between the C-6 position and combined C-11/C-12 positions. Unidentified products are excluded from the analysis; **B** Oxidation of Taxanes using *Tte*UPO mutants in the constructed toolbox. The proportions of the depicted products relative to the total products were determined in a single-step enzymatic reaction. Y-axis Peak area ratio of illustrated compounds in the reaction mixture, with inclusion of unidentified products. Source data are provided as a Source Data file.

In vivo biosynthesis of oxidized taxadiene

Finally, we attempted to construct a biosynthetic pathway for in vivo production of oxidized taxadiene derivatives. Building upon a high-yielding *E. coli* taxadiene production chassis established in our previous work[65], we successfully achieved functional expression of the L208A mutant in *E. coli* through *N*-terminal signal peptide truncation (Supplementary Fig. 14). Subsequent integration of this artificial oxidase module into the taxadiene-producing chassis, coupled with exogenous H_2O_2 supplementation, achieved de novo biosynthesis of taxane oxidation products at a total titer of 14.2 mg/L (Fig. 5).

Discussion

By screening of 29 oxidases, the ability of *Tte*UPO to oxidize the skeleton of taxadiene was revealed. Based on the crystal structure of *Tte*UPO, protein engineering was employed to remodel its substrate channel, enabling precise regulation of both activity and selectivity. Notably, the L208A mutant exhibited a 53-fold improvement in turnover number (TON), resolving the low catalytic activity intrinsic to the wild-type. Leveraging the catalytically promiscuous L60A variant through protein engineering enabled site-directed oxidation of taxadiene. An oxidase toolbox comprising *Tte*UPO mutants was engineered to perform regio- and stereoselective oxidations at C-4, C-6, C-10, C-11, C-12, and C-13 positions of the skeleton of taxanes. This platform establishing a powerful strategy for diversifying oxidation patterns in structurally significant compounds. Finally, we validated the integration potential of this toolbox within the paclitaxel biosynthetic pathway. By truncating the *N*-terminal signal peptide, heterologous expression of the L208A mutant in *E. coli* was achieved, where implementation of a controlled H_2O_2 feeding protocol enabled de novo biosynthesis of oxidized taxadiene derivatives.

In summary, our research establishes steric hindrance within the substrate channel as the principal factor governing both activity and selectivity in *Tte*UPO-catalyzed taxadiene oxidation. While numerous oxidation products remained unidentified due to low production titers, strategic remodeling of the channel of enzyme may enable engineered oxidation at additional taxane sites. Our research demonstrates significant potential as a foundation for the reconstruction of synthetic pathways for paclitaxel and its analogs.

Methods

Strains, genes and vectors

The gene sequences of oxidases were codon-optimized for expression in *Pichia pastoris* (syn. *Komagataella phaffii*) and cloned into the pPICZA vector by GenScript (Shanghai, China). Plasmid cloning was carried out using *Escherichia coli* TOP10 (Novagen, Darmstadt, Germany). *Pichia pastoris* X-33 was employed for the expression of oxidases.

A 6 × His tag was introduced after the signal peptide of *Tte*UPO, with the specific primers detailed in Supplementary Table 1. All primers were synthesized by Tsingke Biotechnology Co., Ltd. (Shanghai, China).

All PCR reactions, including saturation mutation experiments, were conducted using PrimeSTAR® HS DNA polymerase (Takara, Shiga, Japan). The insertion of the 6 × His tag was achieved utilizing homologous recombination assay kits (ClonExpress Ultra One Step Cloning Kit, Vazyme, China).

Shake flask cultivation of the recombinant *P. pastoris* X-33

Shake flask cultivation of the recombinant *Pichia pastoris* was used for the activity screening.

The recombinant *P. pastoris* X-33 strains were cultured for 24 hours in YPD medium containing 100 μg/L zeocin (30 °C, 220 rpm). Subsequently, the strain was inoculated with 1% (*vol/vol*) of the inoculum into 50 mL MD medium (20 g/L peptone; 10 g/L yeast extract; 10 g/L glycerol) and incubated at 30 °C for 16–18 h. After allowing it to stand at room temperature for 4 hours to separate the supernatant and precipitate, 50 mL of induction medium (20 g/L peptone; 10 g/L yeast extract; 13.4 g/L YNB; 100 mM potassium phosphate buffer pH 6.0; 400 μg/L biotin; 200 μM ALA (5-aminolevulinic acid), 3 mM $MgSO_4$) was added to the precipitation. The culture was then incubated with 1% methanol every 24 h for total 72 h.

To confirm that oxidases has been expressed, the activity of the expressed protein was assessed using the substrate ABTS (2,2′-Azinobis (3-ethylbenzothiazoline-6-sulfonic acid) diammonium salt). The assay reaction mixture, containing 1 mM ABTS, 2 mM H_2O_2, and citrate buffer (pH 4.5), was incubated at 30 °C for 1 minute, and the absorbance change at 418 nm was measured (ε418 = 36,000 M^{-1} cm^{-1})[48].

https://doi.org/10.1038/s41467-025-67544-4

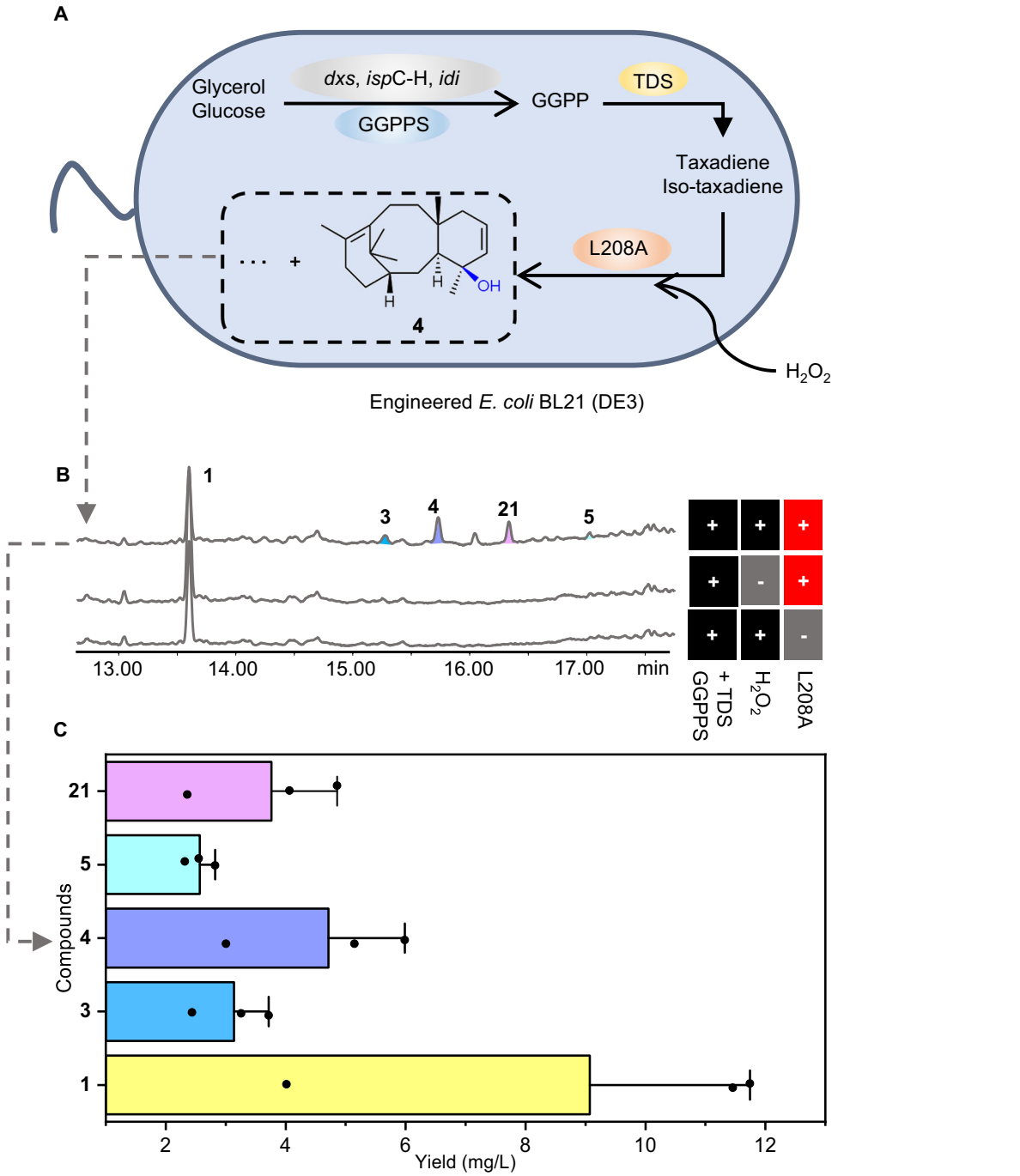

Fig. 5 | De novo biosynthesis of oxidized taxadiene products using an engineered *E. coli* chassis. A Schematic of the biosynthesis pathway of taxadiene oxidation products in engineered *E. coli*. GGPPS: geranylgeranyl pyrophosphate synthase; TDS: taxadiene synthase. H_2O_2 was exogenously supplemented; **B** GC analysis of products from the engineered *E. coli* chassis. Heterologous expression of L208A and exogenous supplementation of H_2O_2 enabled the detection of products **3, 4, 5**, and **21**. **C** Yields of taxane oxidation products in the engineered *E. coli* chassis. The bars are mean of $n = 3$ independent experiments and error bars indicate s.d. Source data are provided as a Source Data file.

Screening of oxidases

29 reported oxidases, with protein sequences and signal peptides consistent with the published literatures, were screened. The expression vector was changed to pPICZA with the AOX1 promoter, and the enzymes were expressed in *P. pastoris* X-33. ABTS was utilized to confirm the correct expression of these oxidase. Subsequently, the expressed oxidases were employed to catalyze the oxidization of taxadiene, with 13 of them demonstrating activity against taxadiene and yielding the same oxidized products (Supplementary Fig. 1 and Supplementary Table 2). *Tte*UPO was chosen due to its highest activity and excellent protein expression level.

The taxadiene oxidation reactions catalyzed by oxidases were conducted at 30 °C in a citrate buffer solution (CPBS) with a pH of 5.5. The reaction mixture contained 0.5 mM taxadiene, 2 mM H_2O_2, 30% (*vol/vol*) acetonitrile, and 50 µL/500 µL concentrated crude enzyme solution was incubated for 1 hour at 200 rpm. Crude enzyme solution was concentrated 50-fold from the fermentation supernatant.

Batch feeding cultivation of recombinant *P. pastoris* X-33

Batch feeding cultivation of *Tte*UPO and its mutants are used for products preparing.

Initial Fermentation Medium: Dissolve 1.14 g/L of $CaSO_4{\cdot}2H_2O$, 14.3 g/L of K_2SO_4, 12.2 g/L of $MgSO_4{\cdot}7H_2O$, 3.3 g/L of KOH, 21 mL/L of phosphoric acid, and 40 g/L of glycerol in deionized water and subject the medium to autoclaving at 121 °C for 20 min. Prior toinoculation, adjust the fermentation pH to 6.0 using ammonia solution and supplement with 12 mL/L of PTM1.

Glycerol Feeding Medium: Dissolve 600 g/L of glycerol in deionized water to a total volume of 400 mL. And subject the medium to autoclaving at 121 °C for 20 min. After cooling, add 4.4 mL/L of PTM1 in a sterile environment.

Methanol Feeding Medium: Add 12 mL/L of PTM1 to pure methanol.

PTM1: Dissolve the following in deionized water in the specified order: 0.2 g/L biotin, 6 g/L $CuSO_4{\cdot}5H_2O$, 0.09 g/L KI, 3 g/L $MnSO_4{\cdot}H_2O$, 0.2 g/L $Na_2MoO_4{\cdot}2H_2O$, 0.02 g/L H_3BO_3, 0.9 g/L $CoCl_2{\cdot}6H_2O$, 42.2 g/L $ZnSO_4{\cdot}7H_2O$, 5 mL/L sulfuric acid, and 65 g/L $FeSO_4{\cdot}7H_2O$. Filter the medium using 0.22 μm filtration to sterilize.

Batch feeding cultivation of *Tte*UPO and its mutants were performed in the following five stage.

Stage 1: Activation of preserved recombinant *P. pastoris* X-33 strains by streaking on YPD plates. Pick single colonies and inoculate into 4 mL of YPD culture medium for 24 h. Inoculate 1% into 250 mL of MD medium and incubate overnight at 30 °C until OD_{600} = 2–6.

Stage 2: In a 5 L tank containing 2.5 L of liquid, use a 10% inoculation rate and incorporate 1 mM final concentration of Ampicillin, and culture at 28 °C. Set up a dissolved oxygen (DO)-stirring linkage, increasing stirring speed when DO < 30% in the range of 200-1200 rpm. Approximately 17–18 h later, there will be a notable increase in DO. Following manually supplementing glycerol, DO will decrease, marking the start of automatic feeding. The DO-STAT system is configured to feeding when DO exceeds 30%, with observed fluctuations maintained around 30% DO. The aeration rate is controlled at 1-2 vvm.

Stage 3: When the OD_{600} reaches a value between 150 and 200, stop feeding. At this point, DO will rapidly increase to a plateau at around 100% and remain steady for about 1 h, ensuring complete consumption of glycerol to prevent any interference with the subsequent methanol induction.

Stage 4: Add 200 μL/L of 1 M ALA, and infuse methanol at a rate not exceeding 7 mL/L/h for a duration of 2 hours to acclimatize the cells to methanol metabolism. Following this acclimation period, configure the DO-STAT to automatically supplement methanol when DO exceeds 30%. The induction culture is maintained for a total of 72 h.

Stage 5: Centrifuge the fermentation broth at 12,000 × *g* for 30 min and collect the supernatant from the fermentation.

Purification of *Tte*UPO

Protein purification was carried out using Ni-NTA. Initially, impurities were eluted using buffer A (20 mM sodium dihydrogen phosphate, 500 mM sodium chloride, pH 7.4) with twice the column volume, followed by elution of *Tte*UPO using buffer B (20 mM sodium dihydrogen phosphate, 500 mM sodium chloride, 50 mM imidazole, pH 8.0) with twice the column volume.

The protein content was determined using the Coomassie brilliant blue method.

Deglycosylation of *Tte*UPO was performed with *Sp*Endo H[66] (mg *Tte*UPO: mg *Sp*Endo H = 5:1). The deglycosylated product was separated by Ni-NTA. Finally, the results of protein purification and deglycosylation were analyzed using SDS-PAGE (Supplementary Fig. 2).

Crystallization and structure determination

The crystallization was carried out at 18 °C in 96-well plates using sitting-drop vapor-diffusion with the commercial crystal condition (1.6% v/v Morpheus III® Dipeptides Mix, 0.1 M Morpheus® -Buffer System 1 pH 6.5, 37.5% Precipitant Mix 4). The droplets consisted of 1 μL of 18 mg/mL purified *Tte*UPO in buffer (10 mM potassium phosphate, pH 7.4) and 1 μL of the precipitant solution and were equilibrated against 50 μL of the precipitant solution. The crystals were flash-cooled in liquid nitrogen for data collection. Diffraction data were collected on beamlines BL10U2 and at Shanghai Synchrotron Radiation Facility. Data were processed with XDS and HKL2000 (Supplementary Fig. 7). The structure was solved by molecular replacement with the structure of *Tte*UPO predicted by AF2[67]. Iterative model building and refinement were performed using WINCOOT 0.9.8.1[68] and PHENIX 1.21.1.5268[69], respectively (Supplementary Table 3).

GC-MS analysis

The analyses were performed with GCMS-QP2010 SE (Shimadzu, Kyoto, Japan), using an HP-5MS fused silica capillary column (30 m, 0.25 mm i. d., 0.50 μm film; Agilent). The oven temperature was from 80 °C to 220 °C (15 °C min^{-1}) and held for 3 min, then by 20 min^{-1} to 280 °C, and held for 5 min. The scan range was set to *m/z* 35-400 and the electron ionization energy was 70 ev.

The reaction mixture was extracted with an equal volume of ethyl acetate, which contained 50 mg/L of octadecane as the internal standard for GC-MS analysis. Standard concentration curve of taxadiene is showed in Supplementary Fig. 3.

The quantitative analysis was performed using GC peak area integration, with the sample size set to $n = 3$. MS was employed for compound identification.

Preparation of taxadiene

The preparation of taxadiene (**1**) follows the established method from our laboratory[65]. After 72 h of induction culture of recombinant *Escherichia coli* BL21 (DE3), the cells were harvested *via* centrifugation, separating the supernatant from the bacterial sediment. The supernatant was subjected to extraction with an equal volume of ethyl acetate, while the bacterial pellet was soaked in an appropriate volume of methanol overnight before being extracted with an equivalent volume of *n*-hexane. The resulting extract was then dried using an appropriate amount of anhydrous sodium sulfate, and the solvent was removed through rotary evaporation at −0.1 Mpa and 30 °C. Preliminary purification of taxadiene was performed *via* silica gel column chromatography, followed by preparative HPLC to isolate taxadiene and its isomers. For the silica gel column chromatography, taxadiene was eluted by *n*-hexane. Detection was performed by TLC, developed with *n*-hexane, and observed by staining with phosphomolybdic acid. The preparative HPLC was conducted using an UltiMate 3000 chrome system (Thermo Fisher Scientific, USA) equipped with an Ultimate ® XB-C18 column (Welch, China). The conditions were set as follows: 100% acetonitrile at a flow rate of 3 mL/min, with detection at 210 nm UV.

Preparation of taxanes

Compound **19, 21**, and **23** were synthesized according to the protocol developed by the Baran's group[15,70].

The synthesis begins with the dibromocyclopropanation of a starting alkene using bromoform ($CHBr_3$) and potassium tert-butoxide (t-BuOK) as base. This resulting cyclopropane intermediate undergoes thermal rearrangement in *N,N*-dimethylaniline ($PhNMe_2$) to form a brominated alkene. In a separate branch, a cyclohexanone derivative is subjected to nucleophilic addition with vinylmagnesium bromide to introduce a vinyl group. The two segments are then converged. The vinyl-functionalized cyclohexanone is deprotonated with *n*-butyllithium (*n*-BuLi) and protected with trimethylsilyl chloride (TMSCl). A key copper(I)-catalyzed conjugate addition is subsequently carried out using methylmagnesium bromide (MeMgBr) in the presence of a copper(II) triflate/N-heterocyclic carbene (NHC) catalyst system. The

resulting enolate is trapped in an aldol reaction with acrolein, and the product is oxidized with Dess-Martin periodinane (DMP) to yield an advanced intermediate. This intermediate is then treated with boron trifluoride diethyl etherate ($BF_3{\cdot}OEt_2$), which triggers Diels–Alder cyclization reaction to form the core ring structure, yielding compound **23** and **21**. The final step is a palladium-catalyzed Negishi coupling between compound **23** and dimethylzinc (Me_2Zn), using tetrakis(triphenylphosphine)palladium(0) ($Pd(PPh_3)_4$) as the catalyst. This coupling installs the final methyl group, affording the desired product (compound **19**) (Supplementary Fig. 13).

Biotransformations

Unless otherwise specified, the biotransformations of taxanes were conducted at 30 °C in a citrate buffer solution (CPBS) with a pH of 5.5. The reaction mixture contained 0.5 mM substrates, 2 mM H_2O_2, 30% (*vol/vol*) acetonitrile, and 40 μg/mL enzyme was incubated for one hour at 200 rpm. The addition of 5 mM 2-hydroxypropyl-*β*-cyclodextrin was found to be beneficial for the biotransformation of taxadiene.

The analytical-grade reaction is conducted in a 2 mL glass injection bottle for a 0.5 mL reaction, whereas the preparative-grade reaction takes place in a 2 L glass shake flask for a 500 mL reaction.

Isotope labeling

Utilizing $H_2{}^{18}O_2$ (Sigma-Aldrich®, Germany) as oxygen donor to oxidize taxadiene, under the conditions described in "Biotransformations" section, the molecular weight of compound **5** shifted from 288 to 290 (Supplementary Fig. 4). This suggests that H_2O_2 serves as the oxygen donor for unspecific peroxygenase during the oxidation of taxanes.

Product preparation and isolation

The reaction system was scaled up to 500 mL and conducted in a 2 L glass shake flask. The supernatant was extracted with ethyl acetate without an internal standard, dried with an appropriate amount of anhydrous sodium sulfate, and concentrated by rotary evaporation at −0.1 Mpa and 30 °C. Subsequently, the resulting product underwent rough separation using silica gel column chromatography. The target compounds were then collected and further purified through preparative HPLC using an UltiMate 3000 chrome system (Thermo Fisher Scientific, USA) equipped with an Ultimate ® XB-C18 column (Welch, China). For the silica gel column chromatography, compounds **2**-**16** were eluted by *n*-hexane: ethyl acetate = 30:1. Detection was performed by TLC, developed with a mixture of *n*-hexane: ethyl acetate in = 6:1, and observed by staining with phosphomolybdic acid. Compounds **17**-**22** were eluted by *n*-hexane: ethyl acetate = 10:1, and its detection was carried out by TLC with a development agent of *n*-hexane: ethyl acetate = 1:1, followed by staining with phosphomolybdic acid. The preparative HPLC conditions are as follows: 100% acetonitrile at a flow rate of 3 mL/min, with detection at 210 nm UV.

Analysis of catalytic mechanism

We synthesized taxadiene-4 (5)-epoxide (**7**) using DMDO[55,56], and analyzed it by GC-MS and ^{1}H NMR as shown in Supplementary Fig. 6.

Synthesis procedure of taxadiene-4(5)-epoxide (**7**): $NaHCO_3$ (12.00 g, 142.85 mmol) was dissolved in a mixture of H_2O (10 mL) and acetone (15 mL). The reaction vessel was placed in an ice-water bath with stirring at 200 rpm. Oxone® (12.5 g total) was added batchwise within 1 min. After stirring for 30 min, the mixture was extracted with diethyl ether (20 mL). The resulting ethereal extract containing DMDO was stored in an ice-water bath. Taxadiene was dissolved in the DMDO/ether solution to a final concentration of 2 mM and reacted with stirring (200 rpm) in an ice-water bath for 1 h. The solvents were removed by rotary evaporation under reduced pressure. Taxadiene-4(5)-epoxide (**7**) was purified using silica gel column chromatography, eluted by *n*-hexane/ethyl acetate (30:1, v/v). Reaction progress and product fractions were monitored by TLC (silica gel, *n*-hexane/ethyl acetate = 6:1, v/v), with visualization achieved by staining with phosphomolybdic acid. The target compound was then collected and further purified through preparative HPLC using an UltiMate 3000 chrome system (Thermo Fisher Scientific, USA) equipped with an Ultimate® XB-C18 column (Welch, China).

Selection of amino acids within the substrate channel

L56, L60, F63, F156, G159, and L208 were selected for the first round of alanine scanning (Supplementary Fig. 8A). It is worth noting that E160 is a conserved site thought to be involved in the oxidation reaction with H_2O_2, and saturation mutagenesis at this position has been significantly diminished the activity.

Building upon the L60A mutant, the following residues were selected for FLA and STY scanning: L56, L59, F63, A155, F156, G159, L208, A163, and the residues M20 and L21 located behind the heme (Supplementary Fig. 8B).

Construction of mutagenesis library

Site-directed mutagenesis was conducted by performing whole-plasmid PCR amplifications of the parental plasmids using PrimeSTAR HS (premix) from Takara along with the respective mutagenesis primers (Supplementary Table 4) carrying the designed mutations. The amplified product was then subjected to digestion with *Dpn* I (NEB) at 37 °C for 2 h to selectively degrade the parental methylated strands. Subsequently, the digested product was transformed into *Escherichia coli* TOP10 cells. For site-directed mutagenesis, an *Escherichia coli* TOP10 colony of the designed mutant was selected from an agar plate and inoculated into 4 mL of LLB medium (containing 5 g/L NaCl, 5 g/L yeast powder, and 10 g/L peptone) supplemented with 100 μg/mL zeocin in a glass tube, and cultivated at 37 °C and 200 rpm. After 12 h of cultivation, the recombinant plasmid was extracted. Linearization of the recombinant plasmid was performed using *Sac* I for 3 h. Linearized fragments were then electro-transformed into *P. pastoris* X33 with a micropulser (BioRad, Hercules, CA, USA). The mutants were cultivated in 250 mL shake flasks containing 50 mL of media (as described in "Shake flask cultivation of the recombinant *P. pastoris* X-33" section).

Site-directed saturation mutagenesis involves mutating a specific site to each of the other 19 amino acids.

Screening of mutants

The mutants were cultivated in 250 mL shake flasks containing 50 mL of media and the secreted supernatant was subsequently purified using Ni-NTA (as described in "Purification of *Tte*UPO" section). The purified enzymes were evaluated for their activity and selectivity through reactions with taxadiene, with the results analyzed via gas chromatography (GC) (as described in "GC-MS analysis" section) (Supplementary Tables 5, 6 and Supplementary Fig. 9-11).

MS, HR-MS and NMR spectroscopy

MS data were measured as described in "GC-MS analysis" section (Supplementary Fig. 15). HR-MS data were measured on a GCT Premier mass spectrometer (Waters Corporation, USA) (Supplementary Fig. 16). HR-MS analysis was performed using dried pure compounds, with a sample size of $n = 1$. NMR spectra were recorded on a Bruker (Billerica, MA, USA) AV Neo 400 MHz, AV Neo 500 MHz, or AV Neo 600 MHz at ambient temperature. Spectra were referenced against solvent signals (^{1}H-NMR, residual proton signal of C_6D_6: $\delta = 7.16$ ppm, CD_2Cl_2: $\delta = 5.32$ ppm; ^{13}C-NMR, signal of C_6D_6: $\delta = 128.06$ ppm, CD_2Cl_2: $\delta = 53.84$ ppm), with a sample size of n = 1. (Supplementary Tables 7–21 and Supplementary Figs. 17–121).

Construction and cultivation of recombinant *E. coli*

L208A codon optimization for *E. coli* was performed at GenScript (Shanghai, China), and the gene was synthesized into the plasmid pET

28a (+). After removal of the *N*-terminal signal peptide, L208A was successfully expressed in *E. coli* and exhibited activity against ABTS and taxadiene (Supplementary Fig. 14A–14F). By optimizing the concentration of the inducer IPTG to 0.1 mM during a 25-h induction, the expression level of L208A was enhanced by over two-fold (Supplementary Fig. 14G). H_2O_2 supplementation was initiated after the first 8 hours of induction and repeated every 8 h (total of 3 additions) When H_2O_2 concentration per addition was kept below 5 mM, bacterial growth was largely unaffected (Supplementary Fig. 14H). Based on these results, we transformed the recombinant plasmid carrying L208A into a taxadiene-producing *E. coli* chassis strain constructed previously in our laboratory (Supplementary Fig. 14I)[65]. The engineered *E. coli* chassis for taxadiene production was designed to overexpress two key upstream enzymes, 1-deoxy-D-xylulose-5-phosphate synthase (DXS) and isopentenyl diphosphate isomerase (IDI), to enhance the supply of the precursors, isopentenyl diphosphate (IPP) and dimethylallyl diphosphate (DMAPP). This elevated precursor pool then enabled the de novo biosynthesis of taxadiene through heterologous expression of geranylgeranyl pyrophosphate synthase (GGPPS) and taxadiene synthase (TS).

The recombinant *E. coli* strain was cultured under the following conditions: A 2% inoculum was transferred into 50 mL of Terrific Broth (TB) medium (12 g/L peptone, 24 g/L yeast extract, 5.2 g/L glycerol, 2.31 g/L KH_2PO_4, 12.54 g/L K_2HPO_4). Initial cultivation was carried out at 37 °C and 200 rpm for 3 h, followed by temperature reduction to 20 °C for 30 min. Subsequently, 0.1 mM IPTG was added, and cultivation continued for another 16 h. Then, 2.5 mM H_2O_2 was added, and cultivation proceeded for an additional 8 h. Finally, the fermentation broth was extracted with an equal volume of ethyl acetate for GC analysis.

Statistics and reproducibility

Unless otherwise specified, all statistical experiments were determined with $n = 3$. No statistical method was used to predetermine sample size. No data were excluded from the analyses. The experiments were not randomized. The Investigators were not blinded to allocation during experiments and outcome assessment.

Reporting summary

Further information on research design is available in the Nature Portfolio Reporting Summary linked to this article.

Data availability

Bioinformatics data; Mutant screening data; Protein crystallization data; GC, MS (EI) and HR-MS chromatograms; and NMR spectra are included in the Supporting Information. Crystallographic data for the structures reported in this Article have been deposited at the Cambridge Crystallographic Data Center, which are available at the CCDC accession 2374527 code (https://www.ccdc.cam.ac.uk/structures/Search?Ccdcid=2374527). Diffraction data for protein reported in this Article have been deposited at Protein Data Bank, which are available at the PDB accession 9IZ8 code (https://doi.org/10.2210/pdb9iz8/pdb). Source data are provided with this paper.

References

1. Holmes, F. A. et al. Phase II trial of taxol, an active drug in the treatment of metastatic breast cancer. *J. Natl. Cancer Inst.* **69**, 341–345 (1994).
2. Bissery, M.-C., Nohynek, G., Sanderink, G.-J. & Lavelie, F. Docetaxel (Taxotere®) a review of preclinical and clinical experience. Part I: preclinical experience. *Anti-Cancer Drugs* **6**, 339–355 (1995).
3. De Bono, J. S. et al. Prednisone plus cabazitaxel or mitoxantrone for metastatic castration-resistant prostate cancer progressing after docetaxel treatment: a randomised open-label trial. *Lancet* **376**, 1147–1154 (2010).
4. Jayanetti, K., Takemura, K., Bendale, H., Garg, A. & Ojima, I. Recent advances in the strategic incorporation of fluorine into new-generation taxoid anticancer agents. *J. Fluor. Chem.* **267**, 110106 (2023).
5. Mohelnikova-Duchonova, B. et al. Hedgehog pathway over-expression in pancreatic cancer is abrogated by new-generation taxoid SB-T-1216. *Pharmacogenomics J* **17**, 452–460 (2017).
6. Seitz, J. D., Wang, T., Vineberg, J. G., Honda, T. & Ojima, I. Synthesis of a next-generation taxoid by rapid methylation amenable for ^{11}C-labeling. *J. Org. Chem.* **83**, 2847–2857 (2018).
7. Denis, J. N. et al. Highly efficient, practical approach to natural taxol. *J. Am. Chem. Soc.* **110**, 5917–5919 (1988).
8. Holton, R. A. Method for preparation of Taxol. EP Patent, EP0400971A2 (1990).
9. Malik, S. et al. Production of the anticancer drug Taxol in *Taxus baccata* suspension cultures: a review. *Process Biochem* **46**, 23–34 (2011).
10. Nadeem, M., Rikhari, H. C., Kumar, A., Palni, L. M. S. & Nandi, S. K. Taxol content in the bark of Himalayan yew in relation to tree age and sex. *Phytochemistry* **60**, 627–631 (2002).
11. Wheeler, N. C. et al. Effects of genetic, epigenetic, and environmental factors on Taxol content in *Taxus brevifolia* and related species. *J. Nat. Prod.* **55**, 432–440 (1992).
12. Holton, R. A. et al. First total synthesis of Taxol. 1. Functionalization of the B ring. *J. Am. Chem. Soc.* **116**, 1597–1598 (1994).
13. Holton, R. A. et al. First total synthesis of taxol. 2. Completion of the C and D rings. *J. Am. Chem. Soc.* **116**, 1599–1600 (1994).
14. Nicolaou, K. C. et al. Total synthesis of taxol. *Nature* **367**, 630–634 (1994).
15. Kanda, Y. et al. Two-phase synthesis of taxol. *J. Am. Chem. Soc.* **142**, 10526–10533 (2020).
16. Hu, Y. J., Gu, C. C., Wang, X. F., Min, L. & Li, C. C. Asymmetric total synthesis of taxol. *J. Am. Chem. Soc.* **143**, 17862–17870 (2021).
17. Min, L. et al. Strategies and lessons learned from total synthesis of taxol. *Chem. Rev.* **123**, 4934–4971 (2023).
18. Ajikumar, P. K. et al. Isoprenoid pathway optimization for taxol precursor overproduction in *Escherichia coli*. *Science* **330**, 70–74 (2010).
19. Zhang, Y. et al. R. Synthetic biology identifies the minimal gene set required for paclitaxel biosynthesis in a plant chassis. *Mol. Plant.* **16**, 1951–1961 (2023).
20. Zhao, Y. et al. Oxetane ring formation in taxol biosynthesis is catalyzed by a bifunctional cytochrome P450 enzyme. *J. Am. Chem. Soc.* **146**, 801–810 (2023).
21. Jiang, B. et al. Characterization and heterologous reconstitution of *Taxus* biosynthetic enzymes leading to baccatin III. *Science* **383**, 622–629 (2024).
22. Liu, J. C.-T., De La Peña, R., Tocol, C. & Sattely, E. S. Reconstitution of early paclitaxel biosynthetic network. *Nat. Commun.* **15**, 1419 (2024).
23. Yang, C. et al. Biosynthesis of the highly oxygenated tetracyclic core skeleton of taxol. *Nat. Comm.* **15**, 2339 (2024).
24. Croteau, R., Ketchum, R. E., Long, R. M., Kaspera, R. & Wildung, M. R. Taxol biosynthesis and molecular genetics. *Phytochem. Rev.* **5**, 75–97 (2006).
25. Jennewein, S., Wildung, M. R., Chau, M., Walker, K. & Croteau, R. Random sequencing of an induced Taxus cell cDNA library for identification of clones involved in Taxol biosynthesis. *Proc. Natl. Acad. Sci. USA* **101**, 9149–9154 (2004).
26. Dejong, J. M. et al. Genetic engineering of taxol biosynthetic genes in *Saccharomyces cerevisiae*. *Biotechnol. Bioeng* **93**, 212–224 (2006).
27. Guerra-Bubb, J., Croteau, R. & Williams, R. M. The early stages of taxol biosynthesis: an interim report on the synthesis and identification of early pathway metabolites. *Nat. Prod. Rep.* **29**, 683–696 (2012).

28. Kaspera, R. & Croteau, R. Cytochrome P450 oxygenases of taxol biosynthesis. *Phytochem. Rev.* **5**, 433–444 (2006).
29. Biggs, B. W. et al. Overcoming heterologous protein interdependency to optimize P450-mediated taxol precursor synthesis in *Escherichia coli*. *Proc. Natl. Acad. Sci. USA* **113**, 3209–3214 (2016).
30. Li, J. et al. Chloroplastic metabolic engineering coupled with isoprenoid pool enhancement for committed taxanes biosynthesis in *Nicotiana benthamiana*. *Nat. Commun.* **10**, 4850 (2019).
31. Mutanda, I., Li, J., Xu, F. & Wang, Y. Recent advances in metabolic engineering, protein engineering, and transcriptome-guided insights toward synthetic production of taxol. *Front. Bioeng. Biotechnol.* **9**, 632269 (2021).
32. Edgar, S., Li, F. S., Qiao, K., Weng, J. K. & Stephanopoulos, G. Engineering of taxadiene synthase for improved selectivity and yield of a key taxol biosynthetic intermediate. *ACS Synth. Biol.* **6**, 201–205 (2017).
33. Yadav, V. G. Unraveling the multispecificity and catalytic promiscuity of taxadiene monooxygenase. *J. Mol. Catal. B-Enzym.* **110**, 154–164 (2014).
34. Song, X. et al. Unraveling the catalytic mechanism of taxadiene-5α-hydroxylase from crystallography and computational analyses. *ACS Catal* **14**, 3912–3925 (2024).
35. Xiao, Z. et al. Cytochrome P450-mediated skeleton rearrangement of taxadiene in an engineered *Escherichia coli* system. *Org. Lett.* **26**, 1640–1644 (2024).
36. McClune, C. J. et al. Discovery of FoTO1 and taxol genes enables biosynthesis of baccatin III. *Nature* **643**, 582–592 (2025).
37. Püllmann, P. et al. A modular two yeast species secretion system for the production and preparative application of unspecific peroxygenases. *Commun. Biol.* **4**, 562 (2021).
38. Püllmann, P. & Weissenborn, M. J. Improving the heterologous production of fungal peroxygenases through an episomal *Pichia pastoris* promoter and signal peptide shuffling system. *ACS Synth. Biol.* **10**, 1360–1372 (2021).
39. Grogan, G. Hemoprotein catalyzed oxygenations: P450s, UPOs, and progress toward scalable reactions. *JACS Au* **1**, 1312–1329 (2021).
40. Hofrichter, M. & Ullrich, R. Oxidations catalyzed by fungal peroxygenases. *Curr. Opin. Chem. Biol.* **19**, 116–125 (2014).
41. Wang, X., Peter, S., Kinne, M., Hofrichter, M. & Groves, J. T. Detection and kinetic characterization of a highly reactive heme-thiolate peroxygenase compound I. *J. Am. Chem. Soc.* **134**, 12897–12900 (2012).
42. Sigmund, M.-C. & Poelarends, G. J. Current state and future perspectives of engineered and artificial peroxygenases for the oxyfunctionalization of organic molecules. *Nat. Catal.* **3**, 690–702 (2020).
43. Ullrich, R., Nüske, J. R., Scheibner, K., Spantzel, J. & Hofrichter, M. Novel haloperoxidase from the agaric basidiomycete *Agrocybe aegerita* oxidizes aryl alcohols and aldehydes. *Appl. Environ. Microbiol.* **70**, 4575–4581 (2004).
44. Peter, S., Kinne, M., Ullrich, R., Kayser, G. & Hofrichter, M. Epoxidation of linear, branched and cyclic alkenes catalyzed by unspecific peroxygenase. *Enzyme Microb. Technol.* **52**, 370–376 (2013).
45. Scheibner, K., Ullrich, R., Kiebist, J., Kellner, H. & Hofrichter, M. Unspezifische Peroxygenasen — Oxyfunktionalisierung außerhalb der Pilzhyphe. *Biospektrum* **26**, 103–106 (2020).
46. Beltrán-Nogal, A. et al. Surfing the wave of oxyfunctionalization chemistry by engineering fungal unspecific peroxygenases. *Curr. Opin. Struct. Biol.* **73**, 102342 (2022).
47. Xu, X. et al. Peroxygenase-catalysed selective oxidation of silanes to silanols. *Angew. Chem. Int. Ed.* **62**, e202302844 (2023).
48. Molina-Espeja, P. et al. Directed evolution of unspecific peroxygenase from *Agrocybe aegerita*. *Appl. Environ. Microbiol.* **80**, 3496–3507 (2014).
49. Rotilio, L. et al. Structural and biochemical studies enlighten the unspecific peroxygenase from *Hypoxylon sp.* EC38 as an efficient oxidative biocatalyst. *ACS Catal* **11**, 11511–11525 (2021).
50. König, R. et al. Novel unspecific peroxygenase from *Truncatella angustata* catalyzes the synthesis of bioactive lipid mediators. *Microorganisms* **10**, 1267 (2022).
51. Gomez de Santos, P. et al. Functional expression of two unusual acidic peroxygenases from *Candolleomyces aberdarensis* in yeasts by adopting evolved secretion mutations. *Appl. Environ. Microbiol.* **87**, e0087821 (2021).
52. Li, T. et al. A novel unspecific peroxygenase from *Agaricus bisporus* var. *bisporus* for biocatalytic oxyfunctionalisation reactions. *Mol. Catal.* **546**, 113275 (2023).
53. Bormann, S. et al. Broadening the biocatalytic toolbox—screening and expression of new unspecific peroxygenases. *Antioxidants (Basel)* **11**, 223 (2022).
54. Domenico, N. K. et al. Recombinant heme thiolate oxygenases. US Patent, US20220282227A1 (2022).
55. Barton, N. A. et al. Accessing low-oxidation state taxanes: is taxadiene-4(5)-epoxide on the taxol biosynthetic pathway?. *Chem. Sci.* **7**, 3102–3107 (2016).
56. Hébert, M., Bellavance, G. & Barriault, L. Total synthesis of ginkgolide C and formal syntheses of ginkgolides A and B. *J. Am. Chem. Soc.* **144**, 17792–17796 (2022).
57. Carro, J. et al. Modulating fatty acid epoxidation *vs* hydroxylation in a fungal peroxygenase. *ACS Catal* **9**, 6234–6242 (2019).
58. González Benjumea, A. et al. Fatty acid epoxidation by *Collariella virescens* peroxygenase and heme-channel variants. *Catal. Sci. Technol.* **10**, 717–725 (2020).
59. Knorrscheidt, A. et al. Accessing chemo- and regioselective benzylic and aromatic oxidations by protein engineering of an unspecific peroxygenase. *ACS Catal* **11**, 7327–7338 (2021).
60. Gomez de Santos, P. et al. Engineering a highly regioselective fungal peroxygenase for the synthesis of hydroxy fatty acids. *Angew. Chem. Int. Ed.* **62**, e202217372 (2023).
61. Münch, J. et al. Computational-aided engineering of a selective unspecific peroxygenase toward enantiodivergent β-ionone hydroxylation. *ACS Catal* **13**, 8963–8972 (2023).
62. Jayadeepa, R. M. & Niveditha, M. S. Computational approaches to screen candidate ligands with anti- Parkinson's activity using R programming. *Curr. Top. Med. Chem.* **12**, 1807–1814 (2012).
63. Wu, T. et al. Reshaping substrate-binding pocket of leucine dehydrogenase for bidirectionally accessing structurally diverse substrates. *ACS Catal* **13**, 158–168 (2023).
64. Yue, D., Ng, E. W. H. & Hirao, H. Hydrogen-bond-assisted catalysis: hydroxylation of paclitaxel by human CYP2C8. *J. Am. Chem. Soc.* **146**, 30117–30125 (2024).
65. Wang, J.-Y. et al. Facile biosynthesis of taxadiene by a newly constructed *Escherichia coli* strain fusing enzymes taxadiene synthase and geranylgeranyl pyrophosphate synthase. *Proc. Biochem.* **122**, 129–136 (2022).
66. Trumbly, R. J. et al. Amplified expression of streptomyces endo-beta-*N*-acetylglucosaminidase H in *Escherichia coli* and characterization of the enzyme product. *J. Biol. Chem.* **260**, 5683–5690 (1985).
67. Jumper, J. et al. Highly accurate protein structure prediction with AlphaFold. *Nature* **596**, 583–589 (2021).
68. Emsley, P. & Cowtan, K. Coot: model-building tools for molecular graphics. *Acta. Crystallogr. D Biol. Crystallogr.* **60**, 2126–2132 (2004).
69. Adams, P. D. et al. PHENIX: a comprehensive Python-based system for macromolecular structure solution. *Acta. Crystallogr. D Biol. Crystallogr.* **66**, 213–221 (2010).
70. Mendoza, A., Ishihara, Y. & Baran, P. S. Scalable enantioselective total synthesis of taxanes. *Nat. Chem.* **4**, 21–25 (2012).

71. Rontein, D. et al. CYP725A4 from yew catalyzes complex structural rearrangement of taxa-4(5),11(12)-diene into the cyclic ether 5(12)-oxa-3(11)-cyclotaxane. *J. Biol. Chem.* **283**, 6067–6075 (2008).

Acknowledgements

We thank Xudong Kong at Shanghai Jiao Tong University for his valuable advice on protein crystallization and structure determination. This work was financially supported by the National Key Research and Development Program of China (2019YFA0905000, Jian He Xu), the Shanghai Commission of Science and Technology (23HC1400200, Hui-Lei Yu) and the National Natural Science Foundation of China (32271540, Hui-Lei Yu and U24A20484, Ran Hong), Shanghai Municipal Science and Technology Major Project (Jian He Xu). Diffraction data were collected at Shanghai Synchrotron Radiation Facility.

Author contributions

Hui-Lei Yu designed the experiments. Mingyuan Lai played a central role in all experiments and completed the majority of the work. Yu Weng, Zhengyu Huang, and Longhao Huang contributed to the preparation and structural analysis of several compounds. Jian Wei, Xin-Yi Lu, and Hangcheng Li assisted with the construction and cultivation of various mutants. Zhijun Zhang, Lili Zhu, Jian-He Xu, and Ran Hong provided valuable support in designing the experiments and offered technical guidance.

Competing interests

The authors declare no competing interests.

Additional information

Supplementary information The online version contains supplementary material available at https://doi.org/10.1038/s41467-025-67544-4.

Correspondence and requests for materials should be addressed to Hui-Lei Yu.

Peer review information *Nature Communications* thanks Zhihua Zhou, and the other, anonymous, reviewer(s) for their contribution to the peer review of this work. A peer review file is available.